Observations of the Lower Atmosphere From the 2021 WiscoDISCO Campaign

Patricia A. Cleary[1], Gijs de Boer[2,3,4], Joseph P. Hupy[5], Steven Borenstein[4], Jonathan Hamilton[2,3], Ben Kies[1], Dale Lawrence[6], R. Bradley Pierce[7], Joe Tirado[1], Aidan Voon[1], Timothy Wagner[7]

[1] Department of Chemistry, University of Wisconsin Eau-Claire, Eau-Claire, WI, 54701, USA
[2] Cooperative Institute for Research in Environmental Sciences, University of Colorado Boulder, Boulder, CO, 80309, USA
[3] Physical Sciences Laboratory, National Oceanic and Atmospheric Administration, Boulder, CO, 80305, USA
[4] Integrated Remote and In Situ Sensing, University of Colorado Boulder, Boulder, CO, 80309, USA
[5] School of Aviation and Transportation Technology, Purdue University, West Lafayette, IN, 47907, USA
[6] Research and Engineering Center for Unmanned Vehicles, University of Colorado Boulder, Boulder, CO, 80309, USA
[7] Space Science and Engineering Center, University of Wisconsin Madison, Madison, WI, 53706, USA

Correspondence to: Patricia A. Cleary (clearypa@uwec.edu)

Abstract. The meso-scale meteorology of lake breezes along Lake Michigan impacts local observations of high ozone events. Previous manned aircraft and UAS observations have demonstrated non-uniform ozone concentrations within and above the marine layer over water and within shoreline environments. During the 2021 Wisconsin's Dynamic Influence of Shoreline Circulations on Ozone (WiscoDISCO-21) campaign, two UAS platforms, a fixed-wing (University of Colorado RAAVEN) and a multirotor (Purdue University DJI M210), were used simultaneously to capture lake breeze during forecasted high ozone events at Chiwaukee Prairie State Natural Area in southeastern Wisconsin from May 21-26, 2021. The RAAVEN platform (data DOI: 10.5281/zenodo.5142491) measured temperature, humidity, and 3-D winds during 2-hour flights following two separate flight patterns up to 3 times per day at altitudes reaching 500 m above ground level. The M210 platform (data DOI: 10.5281/zenodo.5160346) measured vertical profiles of temperature, humidity and ozone during 15-minute flights up to 6 times per day at altitudes reaching 120 m above ground level (AGL) near to a WI-DNR ground monitoring station (AIRS ID: 55-059-0019). This campaign was conducted in conjunction with the Enhanced Ozone Monitoring plan from WI-DNR that included Doppler lidar wind profiler observations at the site (data DOI:10.5281/zenodo.5213039).

1. Introduction

The WiscoDISCO-21 (Wisconsin's Dynamic Influence on Shoreline Circulations on Ozone) was designed to capture lake breeze influence on the shoreline ozone observations and to interrogate the low-altitude dimensionality of the marine layer as it moves on shore. The lake breeze is a mesoscale phenomenon driven by differential air temperatures over land and water surfaces, which in spring and early summer produces a solenoidal circulation in a baroclinic environment that manifests itself as onshore flow during the day. A strong inversion develops as a shallow layer of maritime air is advected onshore and displaces the warmer terrestrial air upward (Holton, 1992; Miller et al., 2003; Martin, 2006; Wagner et al., 2022). These circulations can act as a transport mechanism of emissions on land to over water at night and in early morning hours, then allowing those emissions to not mix when trapped in cooler, temperature inverted air masses over water, eventually being driven back on land through a lake breeze. The goals of the campaign were to: a) characterize lake breeze characteristics of near shore circulation onset and vertical shape along the shoreline of Lake Michigan, b) capture the development or movement of convergence zones/fine scale circulations within the lake-breeze frontal region from offshore to onshore over time and c) monitor ozone gradients, characteristics of chemical circulation patterns within marine-influenced inversions at the shoreline at low altitudes.

The influence of lake breeze on shoreline air quality along Lake Michigan (Keen and Lyons, 1978; Lyons and Cole, 1976; Lyons and Olsson, 1973; Dye et al., 1995; Foley et al., 2011; Stanier et al., 2021) and other Great Lakes (Hayden et al., 2011; Levy et al., 2010; Wentworth et al., 2015; Sills et al., 2011) is well documented by campaigns incorporating ground (Lyons and Cole, 1976), ferry (Lennartson and Schwartz, 2002; Cleary et al., 2015) and aircraft observations (Dye et al., 1995; Foley et al., 2011; Hayden et al., 2011; Stanier et al., 2021). The shoreline communities of Lake Michigan have historically been in non-attainment of federal ozone standards. Precursors to ozone production, volatile organic compounds, (VOCs) and nitrogen oxides (NO_x), have emission sources along the Chicago urban corridor and ozone production can be enhanced when those emissions are trapped in the marine layer over the lake and get transported northward from Chicago (Vermeuel et al., 2019; Dye et al., 1995; Foley et al., 2011). The low altitude features in ozone gradients over Lake Michigan have been observed in the recent 2017 Lake Michigan Ozone Study field campaign (Stanier et al., 2021; Doak et al., 2021). Stanier et al. (2021)

describe observations for the highest measured ozone during the field campaign existing over water, offshore from Milwaukee and in the altitude range of 30-100 m above lake level. Air quality models have been shown to inadequately represent overwater ozone (Cleary et al., 2015; Mcnider et al., 2018; Qin et al., 2019) and do not always capture the ozone gradients at the shoreline (Stanier et al., 2021; Abdi-Oskouei et al., 2020). The shallow marine layer disruption when crossing a shoreline boundary during a lake breeze is a unique environment to study the changes in vertical mixing and pollutant extent.

WiscoDISCO-21featured round-based Doppler lidar observations and two Uncrewed Aircraft Systems (UAS), including the University of Colorado RAAVEN fixed-wing UAS and Purdue University's DJI M210 quadcopter. These platforms were deployed to enhance the level of detail and extend the domains of ground-based measurements to manned aircraft observations with higher spatial resolution and sustained lower-altitude flight. UAS are well suited to make observations of a shoreline environment impacted by a shallow marine layer, where vertical mixing and pollutant transport are key to understanding pollution events at the surface. UAS have been used in riverine environments to highlight pollutant transport and nighttime boundary layer dynamics (Guimaras et al., 2020). During the Ozone Water-Land Environmental Transition Study (OWLETs), UAS, ozone sondes and lidar observations were used to observe ozone titration events above the Chesapeake Bay shipping channel (Gronoff et al., 2019). Horel et al., (Horel et al., 2016) describe the use of distributed ground sensors, tethered sondes and UAS to better understand the meteorological and pollutant transport factors surrounding poor air quality in the Salt Lake Valley. The incorporation of multi-hole probes into fixed-wing UAS has allowed for observations of 3-D winds (Elston et al., 2015) and turbulent fluxes (Wildmann et al., 2014). The RAAVEN platform leveraged in WiscoDISCO-21 has recently been used to study the lower atmosphere across a variety of environmental regimes. This includes nearly a month of flight operations to investigate the thermodynamic and kinematic structure of trade winds over the tropical Atlantic Ocean, (de Boer et al. (2021a) as well as deployments to the US Midwest to make measurements of supercell thunderstorms (Frew et al., 2020). The measurement accuracy of the RAAVEN's instrumentation was recently evaluated at the US Department of Energy's Atmospheric Radiation Measurement (ARM) program's Southern Great Plains facility (see de Boer et al. (2021b) for details).

92

Such high-resolution UAS observations are well-suited for documenting and characterizing the dimensions of the lake breeze phenomenon and corresponding pollutant transport. A combination of UAS and lidar can provide overlapping domains of observations that scale up to the planetary boundary layer, with UAS providing detailed insight into nonuniformities in meteorological observations along the Lake Michigan shoreline. UAS observations are particularly complementary to Doppler lidar observations, as such observations are subject to near-field issues that prevent them from making observations at very low altitudes. Given that the UAS readily operate between the surface and 100 m, these platforms can fill in this gap and provide detailed insight into thermodynamic, kinematic and chemical properties of this layer. These observations have higher vertical and temporal resolution than many chemical models which can provide insight into model resolution issues at the lake-land interface (Wagner et al., 2021). The WiscoDISCO-21 field campaign was conducted in conjunction with the Enhanced Ozone Monitoring initiative from the Wi-DNR who housed added instrumentation for NO, NO_x (NO_x = NO + NO_2) NO_y (NO_y = sum of all reactive nitrogen species), , VOC canisters and PANDORA instrumentation at the Chiwaukee Prairie air monitoring station. The NO, NO_x and VOC measurements can give some indication of the availability of precursors for ozone production and NO_y measurements along with some specific VOCs can indicate something about the past ozone production history of an air parcel. The WiDNR has provided a portal for access to data from these sensors through their web portal (https://wi-dnr.widencollective.com/portals/iwvftorq/AirMonitoringData).

These data sets can be used in a variety of ways to better understand the meteorology and pollution episodes at the Lake Michigan shoreline. The Lidar WindPRO data and RAAVEN data provide complete coverage of the atmospheric dynamics of the marine layer such that it can be characterized and modeled (Wagner et al., 2022; Jozef et al., submitted); Those characterizations could be used to test the fidelity of operational meteorological models (such as HRRR) in modeling the stable boundary layer height. The data sets can also be used to test models for the roughness parameterizations in a shoreline environment using overwater and overland turbulences. The combination of ozone data with the meteorological data can be used to constrain air quality models for the chosen mixing volume for chemical processing in the atmosphere, using the FOAM model (Vermeuel et al., 2019) or testing

120   vertical grid-scale sizing of nested high resolution models for their ability to reproduce the gradients in

121   ozone as measured using UAS (Abdi-Oskouei et al., 2020). The lake breeze phenomenon is similar to

122   bay breeze and sea breeze circulations that complicate modeling efforts in other shoreline locations

123   impacted by poor air quality (Caicedo et al., 2021; Geddes et al., 2021) and model fidelity is crucial to

124   the development of appropriate emissions controls in these environments.

125   **2. Description of Instrumentation and Vehicles**

126   **2.1 University of Colorado RAAVEN UAS**

127   The RAAVEN UAS (Fig. 1) is a fixed-wing UAS with a wingspan of 2.3 m that has been operated by the

128   University of Colorado Boulder since 2019. The RAAVEN's airframe is based on a custom-manufactured

129   model from RiteWing RC. The airframe has been updated to meet the needs of atmospheric science

130   missions spanning a variety of environments. The RAAVEN leverages the PixHawk2 autopilot system

131   and employs an 8S 21000 mAh Lithium Ion (Li-Ion) battery pack to offer flight times around 2.5 hours,

132   depending on conditions and executed flight patterns. Specific modifications to the airframe include the

133   integration of a tail boom to enhance longitudinal stability and improve the platform's performance. The

134   aircraft has a top airspeed of approximately 130 km hr^{-1} , though operations during WiscoDISCO-21 were

135   almost exclusively conducted in the 60-70 km hr^{-1} range.

136
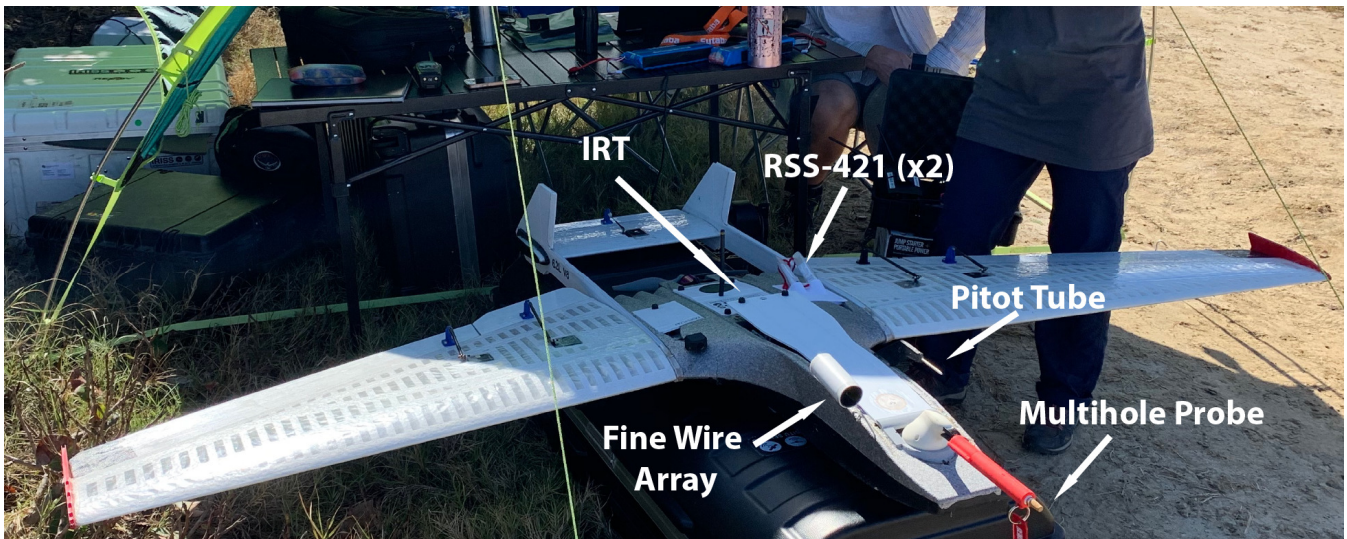
Figure 1: The University of Colorado RAAVEN being prepared for launch during WiscoDISCO21 (top), and a close up of the RAAVEN sensing systems (bottom).

For the WiscoDISCO-21 campaign, the RAAVEN was equipped with an instrument suite derived from the *miniFlux* payload co-developed by the National Oceanic and Atmospheric Administration (NOAA), the Cooperative Institute for Research in Environmental Sciences (CIRES) and Integrated Remote and In Situ Sensing (IRISS) at the University of Colorado. In this configuration, the aircraft was set up to measure atmospheric and surface properties to support evaluation of thermodynamic state, kinematic state, and turbulent fluxes of heat and momentum. This involves a suite of core instrumentation (see Fig. 3), including a multihole pressure probe (MHP) from Black Swift Technologies, LLC (BST), a pair of RSS421 PTH (pressure, temperature, humidity) sensors from Vaisala, Inc., a custom finewire array, developed and manufactured at the University of Colorado Boulder, a pair of Melexis MLX90614 IR thermometers, and a VectorNav VN-300 inertial navigation system (INS). This sensor suite is logged using a custom- designed FlexLogger data logging system.

The Vaisala RSS421 sensors are identical to those used in the Vaisala RD41 dropsonde, and very similar to the Vaisala RS41 radiosonde. This unit employs a linear resistive platinum temperature sensor with a resolution of 0.01 °C, repeatability of 0.1 °C and a response time (as measured within the RS41

157   radiosonde) of 0.5 s at 1000 hPa when moving at 6 m s^{-1}. For relative humidity (RH), the RSS421 includes

158   a thin-film capacitor with a resolution of 0.1% RH and a repeatability of 2% RH, with a temperature-

159   dependent response time of better than 0.3 s at 20 °C (again, as measured within the RS41, with 6 m s^{-1}

160   airflow at 1000 hPa). Finally, the pressure sensor is capacitive with a silicon diaphragm, having a

161   resolution of 0.01 hPa and a repeatability of 0.4 hPa. For WiscoDISCO-21, a pair of these sensor modules

162   was mounted to the top of the RAAVEN's fuselage, between the nose and the tail of the aircraft on the

163   port side. The sensor mounting angles were offset to ensure that the two sensors would have different

164   amounts of solar exposure as the aircraft maneuvers through the atmosphere and to allow for the detection

165   of solar heating effects since no shading is used. Additional information on atmospheric thermodynamic

166   state is available from an E+E EE-03 sensor that is integrated into the BST MHP and from a Sensiron

167   SHT-85 sensor that is integrated in the custom finewire array. The EE-03 has a temperature accuracy (at

168   20 °C) of 0.3 °C, while the humidity accuracy is stated to be 3% RH at 21 °C. The SHT-85 has a stated

169   temperature accuracy of 0.1 °C (from 20-50 °C) and a repeatability of 0.08 C, while the humidity sensor

170   has a stated accuracy of 1.5% RH and a repeatability of 0.15 % RH. Both the EE03 and the SHT-85

171   sensors have slower response times than the RSS421 sensor described above and are typically not used

172   for scientific purposes unless there is a complete failure of the RSS421.

173

174   In addition to the SHT-85 sensor, the finewire array consists of two 5 μm diameter platinum wires

175   extending over a 2 mm length, suspended in the free stream by supporting prongs. One wire is operated

176   as a hotwire anemometer, with approximately 100 °C overheating compared to the ambient environmental

177   temperature. The other wire is operated as a coldwire thermometer, with approximately 1 °C overheating

178   relative to the surrounding environment. The wires have thermal time constants of 0.5 ms in a 15 m s^{-1}

179   airflow regime and support a sampling frequency of up to 800Hz to support measurement of turbulent

180   fluctuations in velocity and temperature. An electronics module converts resistance change in the wires

181   due to velocity or temperature variability to amplified voltages. For WiscoDISCO-21, the finewire was

182   logged at 250 Hz by the FlexLogger, which is equivalent to a 7.2 cm minimum length scale at the

183   RAAVEN's typical cruise airspeed of 18 m s. Time series of these recorded data are processed during

184   post-flight analysis to transform the voltages recorded by the fine wire module to velocity and

185   temperature. Additionally, these measured quantities can be fit to inertial sub-range turbulence models to

186   wavenumber spectra over suitable time intervals, producing turbulence intensity parameters epsilon

187   (kinetic energy dissipation rate) and CT^2 (temperature structure constant). The resolution (noise floor) of

188   these parameterizations is 2.0×10^{-7} W kg^{-1} for epsilon and 4.5×10 K m for CT^2. Resolution of the raw time

189   series are 8.3×10 m s for the hotwire and 1.3×10 K for the coldwire.

190

191   In addition to the EE-03 PTH measurements, the BST 5-hole probe supports measurement of airspeed,

192   angle of attack (α) and sideslip angle (β). These measurements are combined with the GPS-based ground

193   velocities and aircraft attitude from the VectorNav VN-300 to derive the three-components of the inertial

194   wind (u, v, w), as discussed in section 4. The VN-300 can be configured in a dual-Global Navigation

195   Satellite System (GNSS) mode, under which the relative positions of two GNSS antennae are used to

196   calculate the platform yaw. However, this setting was not used during the WiscoDISCO-21 deployment.

197   Under dynamic conditions, the system has a stated accuracy of 0.3 degrees in GPS- Compass heading,

198   0.1 degrees in pitch and roll, 2.5 m horizontal position accuracy, 2.5 m vertical position accuracy when

199   integrating information from the barometric pressure sensor, and 0.05 m s^{-1} accuracy in inertial velocity.

200   Input from the system's gyroscope, accelerometer, GNSS receiver, magnetometer and pressure sensor are

201   filtered through an extended Kalman Filter (EKF) to produce a navigation solution. VN-300 data were

202   logged at 50 Hz resolution during WiscoDISCO-21.

203

204   Finally, RAAVEN deploys two Melexis MLX90614 IR thermometers: one looking up from the top of

205   the aircraft and one looking down towards the surface in level flight. These sensors are factory calibrated

206   to work in operational temperatures between -40 and 125 C, and to measure target brightness temperatures

207   between -70 and 380 °C. They have a high accuracy (0.5 °C) and a measurement resolution of 0.02 °C.

208   The RAAVEN-mounted MLX90614s are not stabilized to maintain a vertical orientation, meaning that

209   the observed target is perpendicular to the reference frame of the aircraft. This requires some care when

210   interpreting measurement from time periods when the aircraft is conducting pitch or rolling maneuvers.

211   For WiscoDISCO-21, we leveraged the "I" version of this sensor which has a 5-degree field of view.

212   These sensors have a broad passband range of 5-14 µm, meaning that while it covers the infrared

atmospheric window, it is also subject to radiation emitted by water vapor and other radiatively active gases, meaning that a significant depth of atmosphere between the aircraft and a given target (e.g., cloud; surface), atmospheric gases influence the temperature reading. Despite this range spanning the 9.6 μm O_3 band, the relative proximity of the sensor to targets of interest (e.g. surface, clouds) means that this overlap is not expected to significantly influence the readings, due to the integrated path length being relatively small. Therefore, if absolute accuracy of brightness temperature is important, the sensor should be operated in close proximity to a target of interest. However, relative contributions from different surface types or atmospheric conditions can still be easily distinguished despite a lack of absolute calibration for extended distance sensing. Such gradient detection can be useful for detecting surface inhomogeneities, or for understanding whether the aircraft is operating under cloud or clear sky.

2.2 M210 UAS

The DJI M210 quad copter was equipped with a 3-D printed top-mounted bracket for holding a 2B Technologies Personal Ozone Monitor (POM) and an Intermet Systems iMET-XQ2 meteorology sensor (Fig. 2). The copter had a ~15 minute flight time with the on-board sensors without a camera. The POM measures ambient ozone using UV absorption and active humidity subtraction by measuring a whole air sample and an ozone scrubbed sample in a 10-s duty cycle. The POM records data to its internal data storage at 10 s interval with a log number and time stamp along with GPS coordinates and instrumentation metrics (optical cell pressure and temperature). The iMET system records temperature, humidity, and pressure along with GPS coordinates and a time stamp to internal data storage. Each instrument (the POM and iMET) had individual data logging systems and separate power supplies. Both the POM and the iMET had GPS capabilities with the POM logging inconsistently and the iMET logging GPS more consistently. Each instrument and the UAS flight recorder logged time stamps. The iMET recorded observations of temperature, relative humidity, humidity temperature and pressure at a frequency of 10 Hz. The POM recorded ozone observations at a frequency of 0.1 Hz. The POM, iMET and M210 time-stamps drifted up to 60 seconds from the other logged data. The flight log recorded the M210 positioning (altitude,

239   latitude, longitude) at 100 Hz. The M210 flight logs, iMET data and POM data were each downloaded

240   separately after each series of flights.

241
242
243
244   **Figure 2**: DJI M210 multirotor UAS with bracket-mounted POM and iMET

245

2.3 Chiwaukee Lidar System

246

247 A Halo Photonics Stream Line XR Doppler lidar (Pearson et al. 2009) was deployed on the roof of the
248 Chiwaukee Prairie air monitoring station (Fig. 3), approximately 3 m AGL. This is the same system that
249 is regularly deployed as part of the Space Science and Engineering Center (SSEC) Portable Atmospheric
250 Research Center, SPARC, (Wagner et al., 2019). The Doppler lidar actively emits pulses of near-infrared
251 radiation at a wavelength of 1.5 μm. This wavelength is long enough that molecular scattering causes
252 little attenuation of the signal, but it is short enough that it is sensitive to aerosols that are suspended
253 within the planetary boundary layer.

254

255 The Doppler lidar uses velocity-azimuth display (VAD) scans of the Doppler lidar to retrieve profiles of
256 wind speed and direction. In VAD, an instrument capable of measuring along-beam velocity (like a
257 Doppler radar or lidar) stares at multiple azimuths at a non-zenith elevation angle over a short period of
258 time, and then reconstructs the profile of winds above the lidar by assessing how the along-beam velocity
259 changes as a function of azimuth and range. For WiscoDISCO-21, the VAD scans were configured with
260 six azimuthal stares per profile (at azimuths of 0 º, 60 º, 120 º, and so on) with an elevation angle of 70 º.
261 Range gates were 18 m. VAD scans were conducted every 4 min and each VAD took approximately 45
262 s to complete. Between VADs, the lidar reverted to vertical stares in order to capture profiles of
263 backscatter and vertical velocity. Since the lidar depends on the presence of scatterers to have a detectable
264 signal return, the depth of the retrieved wind profiles varied significantly throughout the experiment from
265 as shallow as 200 m to as deep as 2 km.
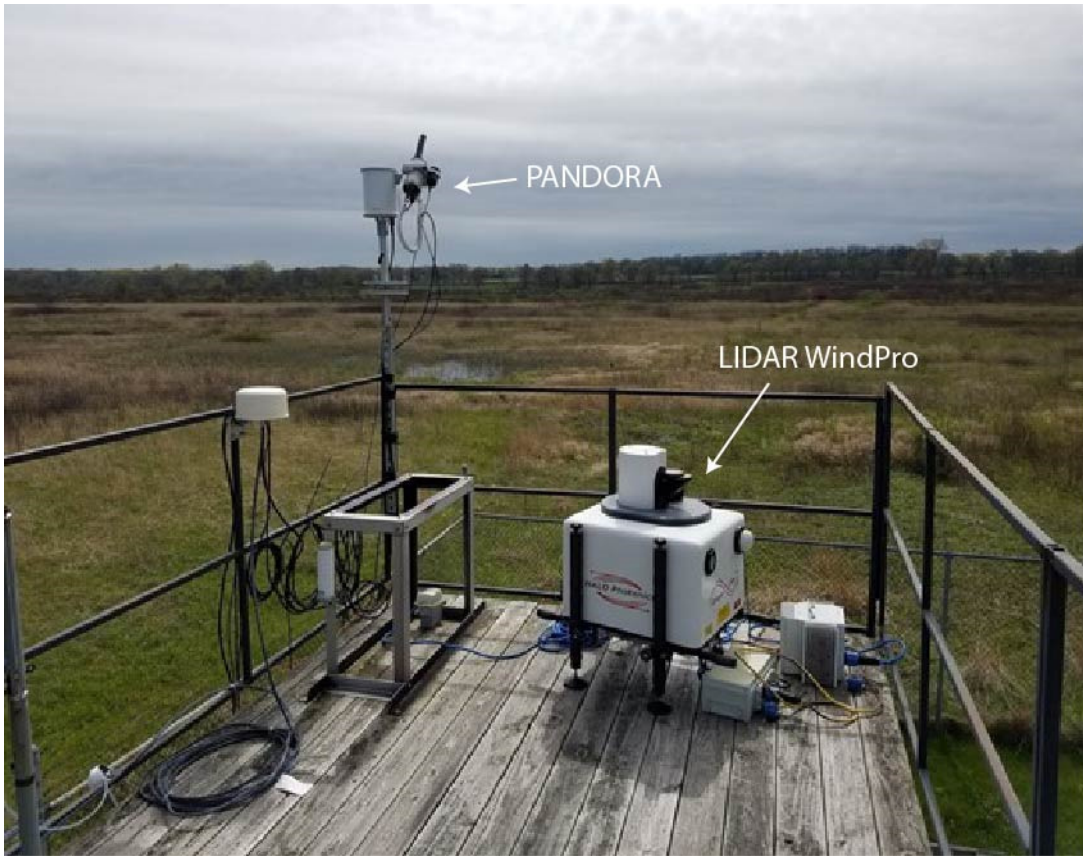
266
267
268 **Figure 3:** Roof of the Chiwaukee Prairie air monitoring system, showing the PANDORA (upper left)
269 and Doppler lidar (right-center). The wooden floor pictured here is approximately 3 m above ground
270 level.

271

272 **3. Description of measurement location, deployment strategies and sampling**

273 The Chiwaukee Prairie State Natural Area is a 485-acre shoreline prairie managed by the Wisconsin

274 Department of Natural Resources (WiDNR) located along the shoreline of Lake Michigan and adjacent

275 to the Wisconsin/Illinois border. The WiDNR operates an air monitoring station (Airs ID 55-059-0019)

276 for Kenosha County within this area, located at 11838 First Court in Pleasant Prairie, WI. This location

277 was chosen due to its suitability for UAS flight operations and the regular influence of lake breeze

278 circulations at the site. As a result of these lake breezes, the WiDNR's Chiwaukee Prairie Monitor

279 regularly observes some of the highest ozone concentrations in the state (Stanier et al., 2021) with a 2015-

280   2017 design value of 78 ppb (Cleary et al., 2022), where the federal ozone standard is 70 ppb for an 8-

281   hour average. Land use in the region is mixed suburban housing and farming, with two marinas directly

282   south of the research site. Chiwaukee Prairie has trail access along Al Kemper Trail and 122nd Street that

283   is isolated from automobile, bicycle and most pedestrian traffic. The M210 flights were conducted near

284   the WiDNR Air Monitoring site (Latitude: 42.5045, Longitude: -87.8095) and the RAAVEN flight

285   operations were conducted on Al Kemper Trail or 122nd St to provide ample room for take-off and

286   landing (Fig. 4).

287
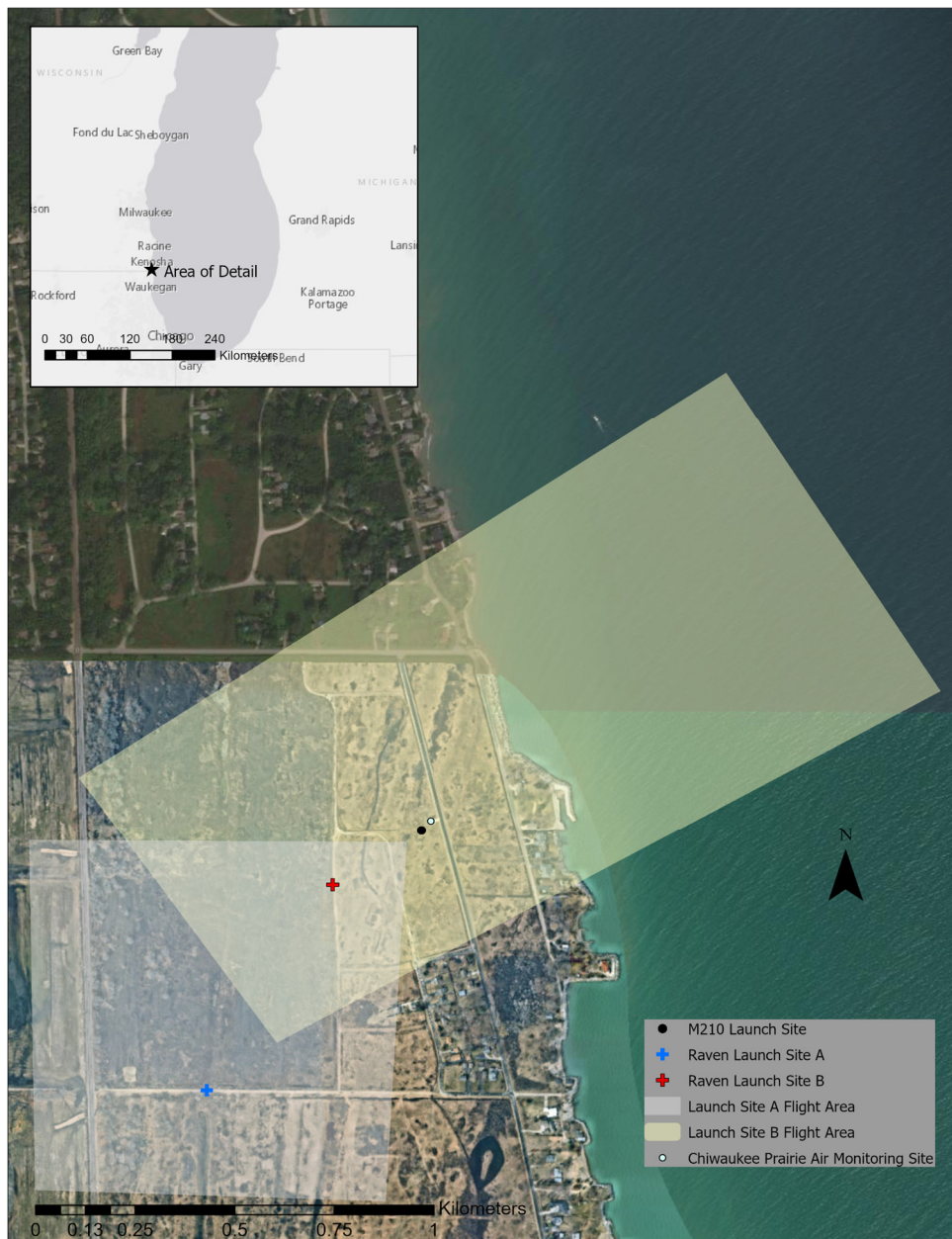
Figure 4: Research site map including Chiwaukee Prairie air monitor and locations for launch sites for M210 and RAAVEN. Map created using Esri ArcPro version 2.52 using ArcPro basemap imagery.

The primary goal for the field campaign was to capture elevated ozone concentration events resulting from lake breeze circulations at the site. The deployment strategy for selecting a time window for field

operations was dictated by ozone and meteorological forecasts that predicted light southerly winds for an extended period that would both a) increase the likelihood of onshore lake breeze flow from weaker southerly winds and b) drive pollutant transport from the Chicago metro area to the site.

Forecasts from both the WiDNR and Realtime Air Quality Modeling System (RAQMS) were used to select an ideal deployment period. The dates of May 21-26, 2021 were chosen as meeting those requirements. The selection of the time period for the campaign was dictated by capturing a combination of lake breeze and ozone events. An acceptable window for operations from late May 23 through mid-June was targeted because of the higher frequency of high ozone and lake breeze events occurring in this region during late spring/ early summer (see Cleary 2022, SI for a list of high ozone events for the years 2013-2019 at Chiwaukee Prairie). Once the operations window was approaching, the team used the RAQMS forecast model (Fig. 5) and consulted with the Wisconsin Department of Natural Resources (WiDNR) Air Quality Division's meteorologist to decide on a "go time" to initiate deployment from all collaboration partners for an 8-day campaign. The go time required evidence that synoptic flow would have a southerly component for a few days (normally brought about by a high-pressure system over the Ohio River Valley) with limited precipitation events. Flights were canceled during days in which high ozone or southerly/southeasterly lake breeze were not expected (Table 1).

312
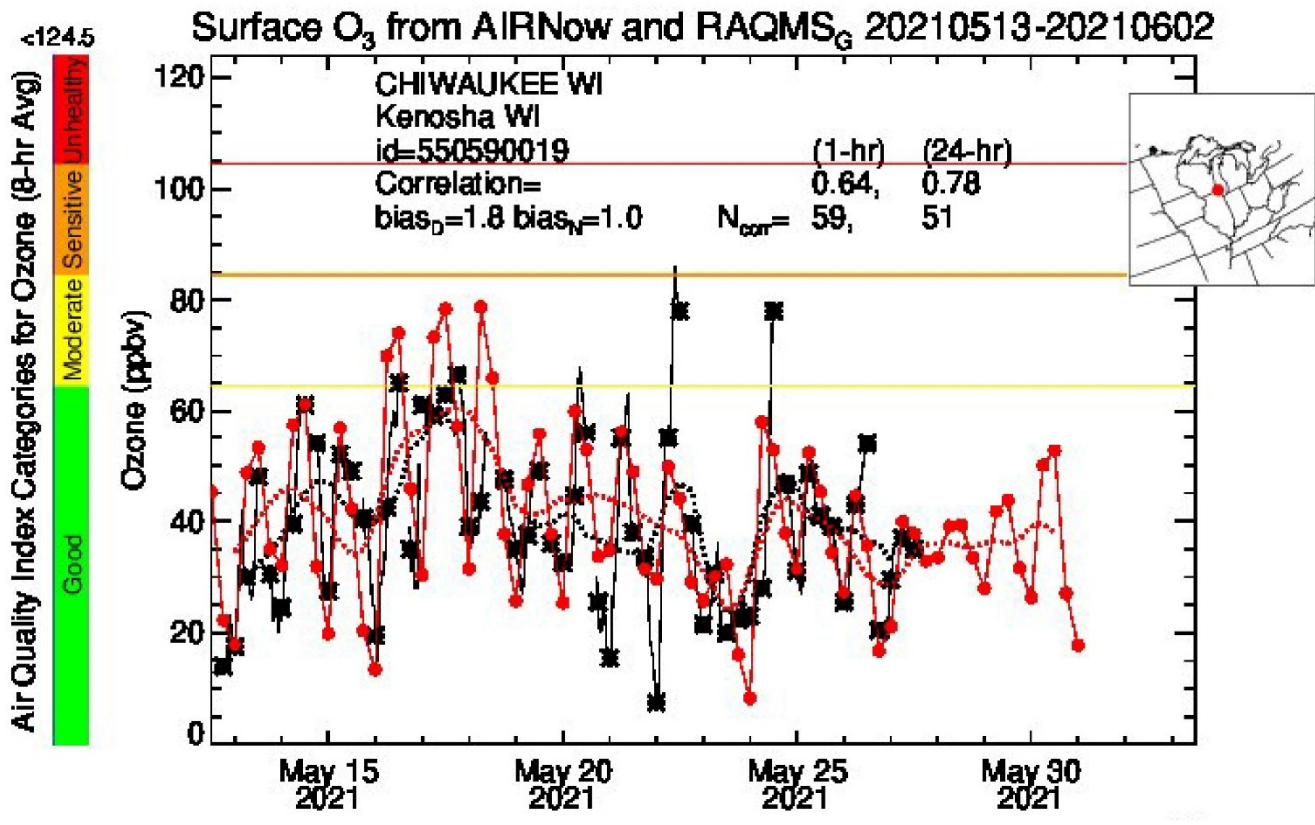
Figure 5: 8-hour ozone concentrations from RAQMS forecast (red) and observations (black) for May 13-

314   26, 2021 at Chiwaukee Prairie.

315

Table 1: UAS flight days and conditions for the WiscoDISCO-21 field campaign. Flight Pattern A and

317   B are depicted in Figure 2 A.

318

Date (2021)	M210 (time UTC)	University of Colorado RAAVEN (Time UTC and flight pattern)	Weather and Air Quality Conditions
Friday, May 21	F1 (15:35-15:44) F2 (16:38-16:47) F3 (19:08-19:21) F4 (19:46-19:59)	F1 (15:01-16:54) Pattern A F2 (18:36-20:40) Pattern A	SW wind, Temps > 25 $^{\circ}$C, small shift in winds to colder from SSE

Saturday, May 22	F1 (14:22-14:35) F2 (15:18-15:31) F3 (17:27-17:41) F4 (18:26-18:41) F5 (20:09-20:22) F6 (20:59-21:14)	F1 (13:52-15:55) Pattern A F2 (17:00-19:03) Pattern A F3 (19:30-21:38) Pattern A	W wind in AM, Temps > 25 $^{\circ}$C, consistent shift in winds to colder from SSE.
Sunday, May 23	no flights	no flights	W to NE winds, dropping temperatures, AM showers, PM showers
Monday, May 24	F1 (15:08-15:23) F2 (16:01-16:16) F3 (18:14-18:29) F4 (19:12-19:27) F5 (21:09-21:19) F6 (22:04-22:19)	F1 (14:24-16:30) Pattern B F2 (17:41-19:50) Pattern B F3 (20:42-22:51) Pattern B	S winds, lake breeze, high ozone event (> 70 ppb).
Tuesday, May 25	F1 (14:00-14:15) F2 (14:49-15:04)	F1 (13:39-15:42) Pattern B	SW winds, slight lake breeze in the morning, overtaken by westerlies
Wednesday, May 26	F1 (13:43-13:58) F2 (14:37-14:52) F3 (16:47-17:02) F4 (17:47-18:01) F5 (19:51-20:06) F6 (20:48-21:01)	F1 (13:27-15:24) Pattern B F2 (16:31-18:20) Pattern B F3 (19:30-21:22) Pattern B	W wind, steady all day, sunny. After all flights, lake breeze came in from NE

319
320
321

322   Flights were conducted in the time window 08:00-17:00 local time, CDT (13:00-22:00 UTC) (Table 1).

323   The RAAVEN platform features 2-hour flight times and was deployed to complete up to 3 flights per

324   day. The M210 flew slow ascents to 120 m AGL with an approximate 15-minute flight time, completing

325   up to 6 flights per day and the sampling pattern was designated to achieve maximum overlap with the

326   RAAVEN flight times by conducting two flights per RAAVEN flight.

327

328

During WiscoDISCO-21, the RAAVEN completed 12 flights, totaling 25.4 flight hours, operating under

a Certificate of Authorization (COA) from the US Federal Aviation Administration (FAA) to allow flights

up to 518 m AGL. Fig. 6a shows a map of the RAAVEN flights, while figure 2b includes a histogram of

the altitudes covered by these flights. Flights were designed to follow two distinct flight patterns A and

B to capture over-prairie profiles using a circular pattern with holding at altitudes 400, 250, 150, 100 and

50 m AGL and over-water/over-prairie profiles using an extended racetrack pattern that traversed the

shoreline, with holding altitudes at 400, 250, 150, 100 and 50 m AGL (see Figure 6c for the two flight

patterns). Figure 7 shows histograms of the measurements obtained by the RAAVEN over the length of

the campaign, including temperature, relative humidity, wind speed, wind direction, air pressure, and

surface and sky brightness temperature.
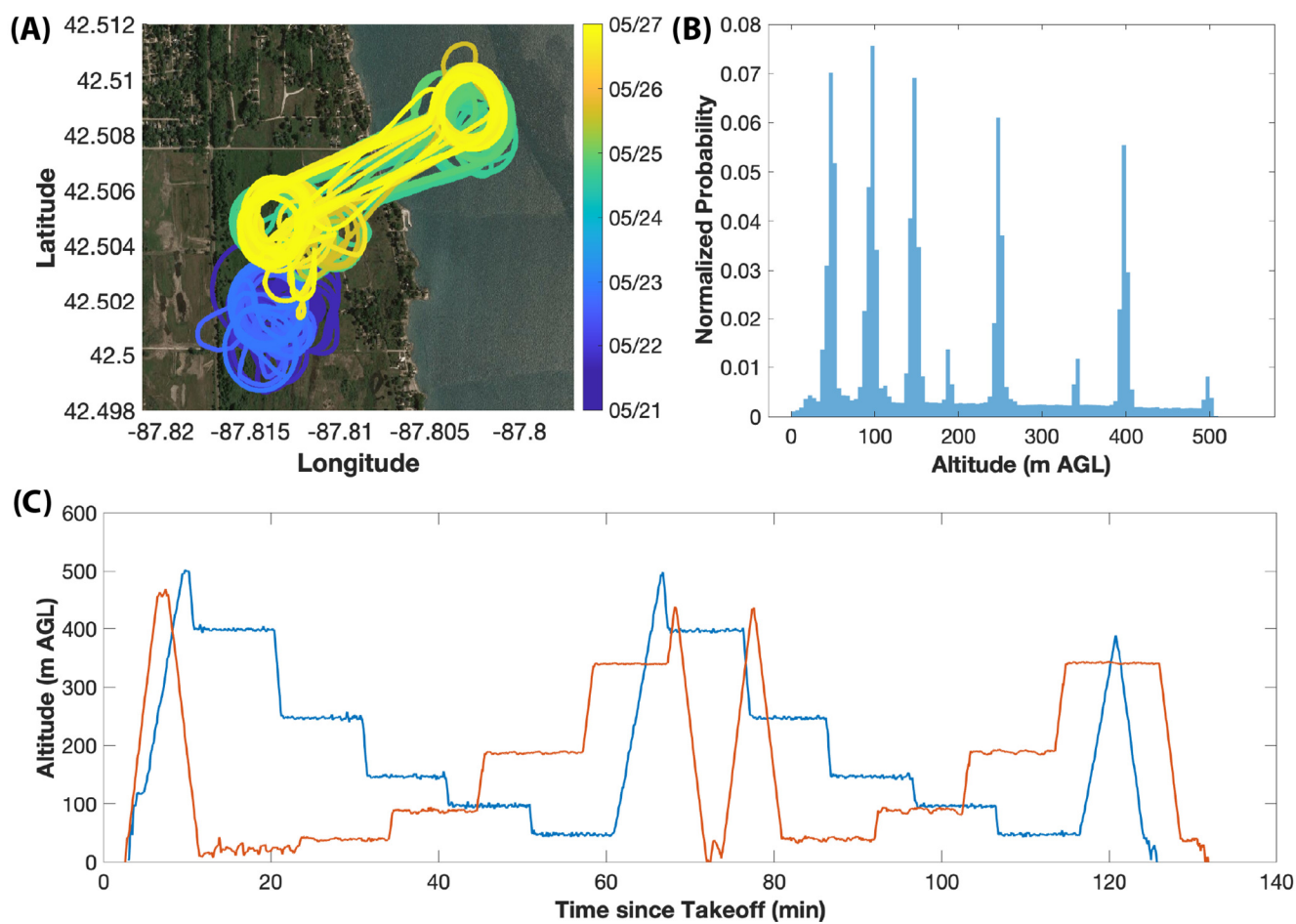
339

340   **Figure 6:** A map showing the flight tracks for the RAAVEN with blue showing flight pattern A and
341   yellow or green showing flight pattern B (a), a histogram of altitudes sampled by the RAAVEN (b), and
342   example time-height plots of the two types of RAAVEN flights (c). The "normalized probability"
343   presented for a given bin is the number of elements in a given bin divided by the total number of elements
344   in the input data, so that the integral of the histogram equals one. Background maps are © GoogleMaps
345   2021, downloaded through their API.
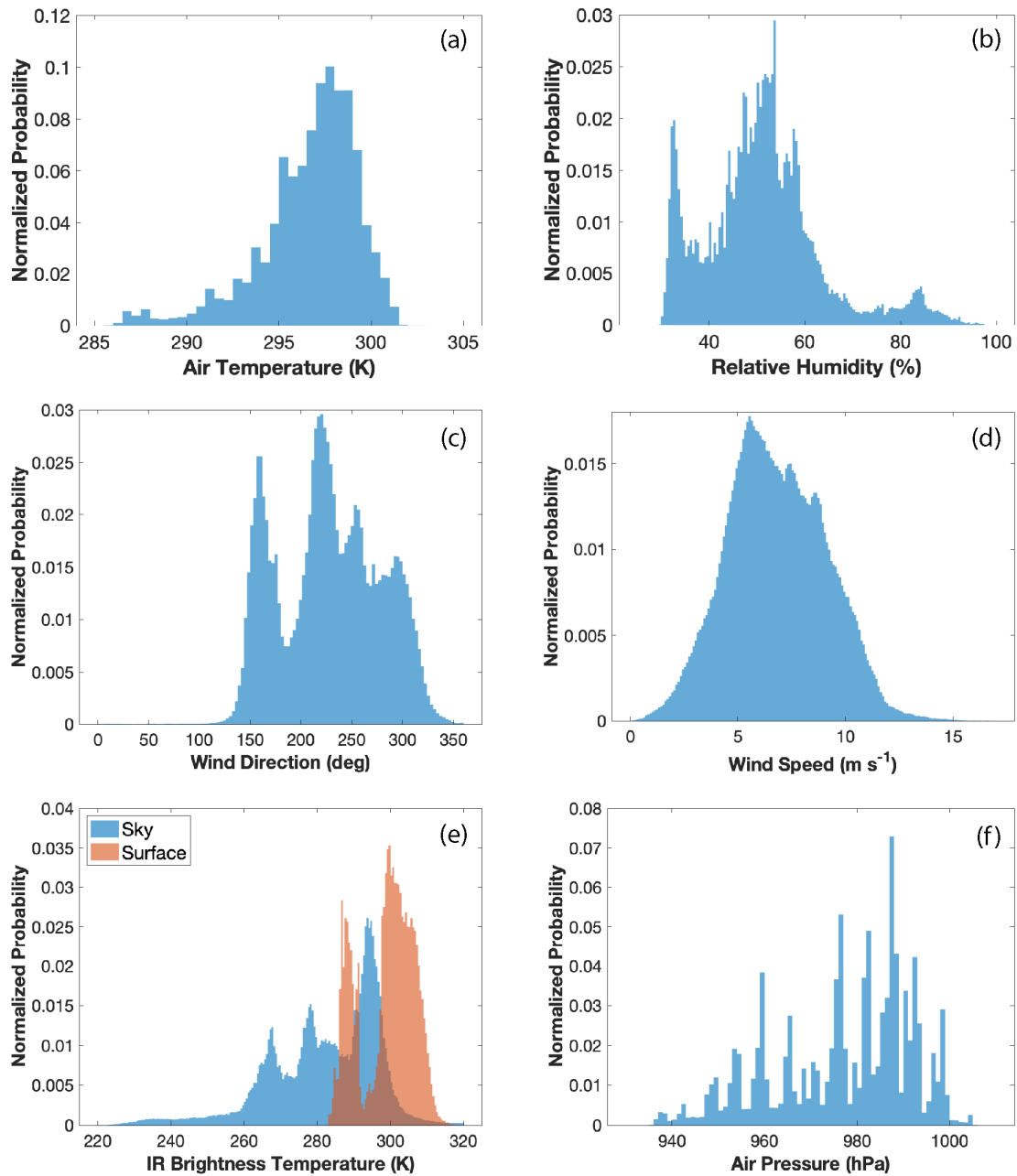
Figure 7: Histograms of (a-f) temperature, relative humidity, wind direction, wind speed, IR brightness temperatures, and air pressure, as measured by the RAAVEN during WiscoDISCO-21. As in figure 6, the "normalized probability" presented for a given bin is the number of elements in a given bin divided by the total number of elements in the input data, so that the integral of the histogram equals one.

351   **4. Data processing and quality control**

352   **4.1 University of Colorado RAAVEN UAS**

353   Data collected by the different sensors carried by the RAAVEN during WiscoDISCO-21 were logged at

354   a variety of different logging rates. The finewire system was logged at 250 Hz, the fastest rate of all of

355   the sensors. The BST MHP was logged at 100 Hz, the VectorNav VN-300 at 50 Hz, the Melexis IR

356   sensors and variables related to finewire status were logged at 20 Hz, while data collected from the

357   PixHawk autopilot and Vaisala RSS421 sensors were logged at 5 Hz. Each logging event carried out by

358   the FlexLogger includes a sample time from the logger CPU clock, allowing for post-collection time

359   alignment between the different sensors. These sample times, along with artificial 5, 20, 50, 100, and 250

360   Hz clocks spanning the sample times between initial GPS lock and the last recorded sample time for the

361   VN-300, are used to align the different variables to a set of common clocks, primarily through one-

362   dimensional linear interpolation. One exception to the linear interpolation is the yaw estimate, which is

363   circular in nature (ranging between -180 and 180 degrees), and therefore uses a "nearest" interpolation to

364   ensure that the transition from 360 to 0 degrees is not represented as 180. During this interpolation

365   process, a limited number of points sharing a common sample time with another point are removed from

366   the record. Once these time variables are established, a *base_time* variable is established using the 250

367   Hz time stamp, and offsets from *base_time* are then calculated for all different logging resolutions.

368

369   The resampled (in time) dataset includes a variety of derived and measured quantities. Aircraft position,

370   including latitude, longitude, and altitude, are measured by the VN-300. The aircraft altitude is corrected

371   using a combination of various inputs from onboard GPS and pressure altimeters, as neither of these

372   altitude estimates can be used reliably as a definite flight altitude. Pressure altitude is subject to drift over

373   the duration of a single flight due to atmospheric evolution over a 2.5-hour window, potentially resulting

374   in values at landing that are higher or lower than those at take-off. Similarly, the accuracy of the GPS

375   altitude is insufficient to capture the vertical position of the aircraft to the level of detail required. To

376   calculate a true altitude, a combination of the autopilot altitude, VN-300 altitude, and VN-300 pressure

377   are used. First, a *flight_flag* variable is computed using airspeed and altitude information from the

378   autopilot. Any data points with airspeed exceeding 10 m s^{-1} and an altitude exceeding 5 m AGL is flagged

379   as a time when the aircraft is flying (*flight_flag*=1). The point at 200 samples (4 seconds) prior to the

380   first point in the record where the aircraft is deemed to be flying is recorded as the initial take-off index,

381   while the data point at 200 samples (4 seconds) after the last point in the record where the aircraft is

382   deemed to be flying is recorded as the landing index. The difference between the autopilot altitude at

383   these two indices is added into the flight record on a timestep-by-timestep basis, to correct for temporal

384   drift in pressure. A linear fit is then calculated to relate the VN-300 pressure and the difference between

385   the VN-300 reported altitude and the autopilot reported altitude. This pressure-dependent altitude

386   correction is then applied to the VN-300-reported altitude to derive a final altitude.

387

388   Wind estimation from fixed-wing aircraft requires the combination of several different measurements

389   related to airspeed, aircraft motion, and airflow over the aircraft (see van den Kroonenberg et al., 2008).

390   These measurements need to be of sufficient quality, and angular offsets and logging delays need to be

391   considered and removed. For RAAVEN, true airspeed (TAS) biases have a large impact on derivation of

392   wind speed, while the angular offsets between the MHP and INS and time-lag between the GPS and in

393   situ measurements have smaller impacts. These potential sources of error are corrected for using an

394   optimization technique, where small adjustments are made to the individual parameters and the

395   combination that results in the wind solution with the smallest overall variance is selected as the correct

396   winds.

397

398   For the RAAVEN WiscoDISCO-21 dataset, TAS is calculated using measurements from the MHP and

399   RSS421 probe using equation 1 from (Brown et al., 1983):

$$TAS_i = \sqrt{\frac{2\bar{q}}{\rho}} \tag{1}$$

401   where ρ is the density of air calculated using the static pressure reported from the MHP, temperature from

402   the RSS421, and the specific gas constant for dry air, $\bar{q}$ is defined as:

$$\bar{q} = \frac{p_0}{1 - \frac{9}{4}\sin^2 \theta_a} \tag{2}$$

404   where $\sin^2 \theta_a$ is the total aerodynamic angle of the MHP, calculated using the angle of attack (α) and

405   sideslip angle (β) reported by the MHP.

Based on testing in a temperature chamber, the pressure sensors used in this version of the MHP were found to have non-linear temperature dependencies. This requires the application of an additional temperature-dependent correction to ensure that an artificial alteration of TAS with altitude was not present. Additional information on the calculation of airspeed and other quantities from the MHP can be found in (de Boer et al., 2021a).

Derivation of the RAAVEN's thermodynamic measurements included multiple processing steps. First, data from the two RSS421 sensors are averaged to attempt to reduce the influence of any solar exposure of the sensors. Previous evaluations of the potential for solar contamination have not revealed any specific biases on the observation (see de Boer et al., 2021a). Over the course of the WiscoDISCO-21 campaign, the two sensors varied by less than 0.5 °C (Fig. 8). The averaged temperature time series was then used to calibrate the coldwire data by applying a linear fit to the relationship between the coldwire voltage and the temperature measured by the RSS421 sensor. The RSS421 relative humidity values were also averaged. Typically, the RH measurements agreed to within 2%.
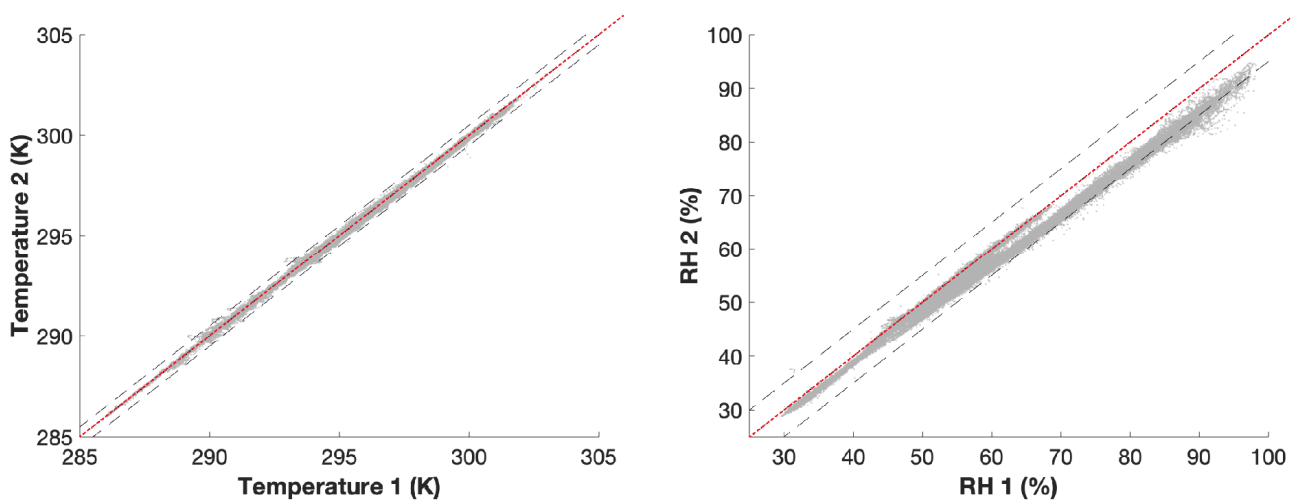
Figure 8: A comparison of temperature (left) and relative humidity (right) observations from the two Vaisala RSS-421 sensors on RAAVEN for all flights. The red dotted lines represent a one-to-one agreement, with the dashed black lines representing 0.5 degree (for temperature) and 5% (for relative humidity) deviation from perfect agreement.

428 All quantities measured by the RAAVEN have data quality flags associated with them. For the RSS421-
429 derived temperature, the flag is set to zero for good data, and set to one for times when any of the following
430 occur: a) the absolute value of the difference between the temperature from either individual sensor and
431 the output temperature is greater than 0.5 °C, b) the absolute value of the difference between the output
432 temperature and the temperature from the EE-03 sensor on the MHP exceeds 5 °C, c) the recorded error
433 flag of either RSS421 sensor is active, or d) the aircraft is not flying. For the RH measurement from the
434 RSS421, a similar set of criteria are used to activate the data quality flag, except the limits are set to be
435 6% between RSS421 sensors, and 15% between the output RH value and the MHP-provided RH value.
436 The relative humidity values from the MHP are significantly impacted by the exposure of that sensor to
437 sunlight and the associated impact on sensor temperature. This is not corrected for, resulting in large
438 fluctuations in the RH values at times. As a result, this measurement (from the MHP) only provides a
439 reality check to ensure that the RSS421 are reporting accurate values, and therefore such a large offset
440 (15%) is allowed. The more important comparison is between the two RSS421 sensors, which should
441 agree much more closely, as they are the same sensor type, and are mounted within close proximity of
442 one another. The coldwire temperature data quality flag is activated when the difference between the
443 coldwire temperature and either of the RSS421 temperatures exceeds 1 °C, when the absolute value of
444 the difference between the coldwire temperature and the MHP temperature exceeds 3 °C, when the
445 coldwire voltage is observed to fall outside of the 0-4 V analog range, or when the aircraft is not flying.
446 Finally, the pressure quality control flag for the pressure measurement from the VN-300 is activated if
447 the absolute value of the difference between the reported VN-300 static pressure and that measured by
448 either of the RSS421 sensors exceeds 2.5 hPa. The RSS421 pressure measurements are not used because
449 they are believed to be biased low due to the airflow passing over their location on the aircraft.

451 In addition to the flags discussed above, we include a 3-stage flag for the wind measurements, which is
452 set to 0 (good data), 1 (suspect data) or 2 (bad data). Data are determined to be bad if any of the following
453 conditions were met:

454   -   The measured angle of attack or sideslip exceeds 20 degrees, with values between 10-20

455   degrees are flagged as "suspect"

456   -   The true airspeed (TAS) is below 10 m s^{-1}

457   -   Any of the MHP ports are deemed to be blocked, as determined by the differential pressure

458   value for any of the sensors falling below -100 Pa

459   -   The moving window variance of the MHP-derived TAS over 40 seconds is less than 5

460   -   The aircraft is not flying

461   -   The difference between the MHP TAS and that from the Pitot probe is greater than 5 m s^{-1}

462

463 Finally, we included two additional flags in the datastream to allow data users to better understand aircraft

464 flight state and support sampling during specific phases of flight. These flags include the "Flight_Flag"

465 introduced previously, as well as a "Flight_State" flag. The "Flight_State" flag includes information on

466 whether the is flying straight (0) or is turning (1) in the ones place, whether the aircraft is descending (0),

467 level (1), or ascending (2) in the tens place, and whether the aircraft is in flight (1) or not (0) in the

468 hundreds place. If, for example, a data user wanted to analyze straight, level flight legs, they would search

469 for data with "Flight_State" equal to 110. These flags are derived from information from a combination

470 of sensors, including the altitude variable described above, the aircraft yaw, and the "Flight_Flag" variable

471 described earlier on in this paragraph.

472

473 The accuracy of the RAAVEN observations has been evaluated in previous studies. For example, a

474 comparison of RAAVEN data with measurements collected by radiosondes launched from the Barbados

475 Cloud Observatory was conducted in recent work from de Boer et al., (2021b). While radiosondes in that

476 evaluation were launched approximately 20 km to the southeast, the air sampled by both systems was

477 largely representative of the marine boundary layer, implying limited spatial variability. In that

478 evaluation, the observations from the RAAVEN were very well correlated with those from the

479 radiosondes and do not show any positive or negative bias, supporting the idea that the RAAVEN

480 measurements provide an accurate depiction of the lower atmosphere. In addition, recent work allowed

481 for direct comparison of RAAVEN data to observations collected by radiosondes and a 60 m tower at the

482   US Department of Energy's Southern Great Plains (SGP) research site. That study, de Boer et al. (2021a),

483   similarly provided confidence in the RAAVEN observations, showing close statistical agreement between

484   the different data sources.

485

486   **4.2 M210 UAS**

487   Data from the M210 flight controller, the POM and the iMET were all logged to individual instrument

488   internal data storage with independent timestamps. The average flight time of the M210 was 13.96 min.

489   The POM instrument logged data at 0.1 Hz. The iMET logged data every 10 Hz and the M210 flight log

490   recorded UAS GPS positioning and flight statistics at 100 Hz. The ozone concentrations from the POM

491   are adjusted to calibrated values, where ozone calibrations were conducted before every set of 2 flights

492   for the M210 using a 2BTech Model 306 ozone calibration source (Fig. 9). Data quality flags are

493   established as 0 = no concern, 1 = time flag, 2 = calibration and time flag. The time flag indicates flights

494   where the time offset between the M210 and the instrument time offset is large (iMET > 10 s or POM >

495   30 s). The calibration flag indicates when the POM was not responsive to the ozone calibration source

496   (Flight 5 on May 24) after an over-water flight. All times were averaged to 90 seconds and compressed

497   to the time window of observations for a single M210 ascent using the M210 timestamp. A time stamp

498   for 90s averaged data from all instrumentation on the M210 was generated by using the M210 timestamp

499   as primary and adjusting to a time offset in either the POM or the iMET for the start of a flight, then

500   averaged each variable for every 90 second interval of the flight. A 1σ standard deviation is presented as

501   the uncertainty for the 90-s averages. The iMET observations of temperature, relative humidity, pressure

502   and humidity temperature are presented using the 90-s averages with uncertainty as 1σ standard

503   deviations. Each flight ascent start and end were determined by observed changes in atmospheric pressure

504   by the iMET sensor, altitude change in the M210, or noted time of ascent in field notebook for the POM.

505   The altitudes for each observation were obtained by averaging the M210 flight log altitude data for the

506   90-s timestamps. The flight data timestamps varied slightly for each data source. The POM time drift was

507   the most pronounced, with an average difference between the iMet of ~ 24 s. The POM's time was

508   adjusted manually throughout the campaign as the time would drift over the course of one flight. The

509   average difference between the iMet and the M210 over 20 flights was ~ 4 s. Only 20% of flights had a

510   time-difference between iMET and M210 greater than 10 seconds. Instrument battery loss occurred for

511   the iMET system which resulted in lost data for a 2flights on May 26, 2021.
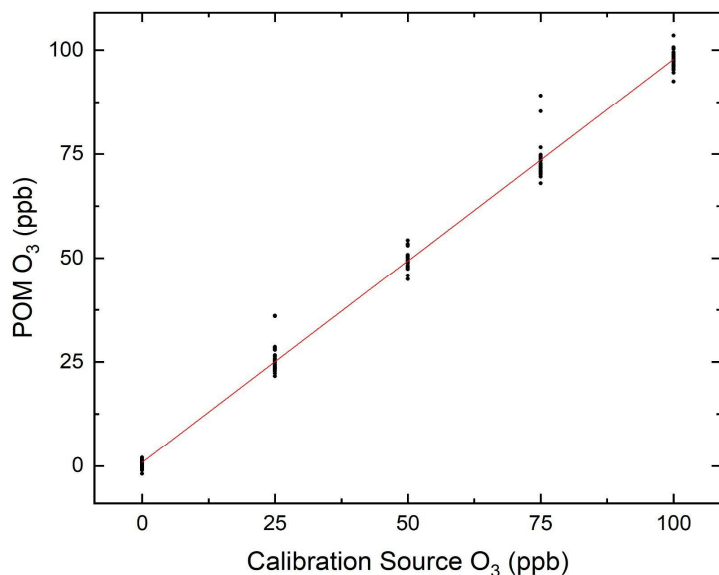
512
513   **Figure 9**: A sample POM calibration from May 24, 2021. The linear regression fit gives: $y = 0.9689$ ($\pm$

514   0.0061) $x + 0.83$ (±0.35), $R^2 = 0.9937$. Each calibration concentration had a 5-minute duration with the

515   POM logging 10-s data.

516

517   Intercomparison between observations made via instrumentation on the M210 at 5 m AGL and at the Wi-

518   DNR ground station show a linear agreement between the observations (Fig. 10). The linear agreement is

519   better for the iMET temperature and the ground station temperature with $R^2 = 0.970$ in comparison to R^2

520   $= 0.955$ for O_3 observations. The O_3 linear fit, $O_{3\ (POM)} = 0.944$ ($\pm$ 0.044) $O_{3\ (DNR)}$ - 3.3 (±1.9), has a

521   negative intercept. The uncertainties in the POM's O_3 concentrations are much larger than uncertainties

522   in the ground station instrumentation. The linear agreement between the different instrumentation on

523   separate observation platforms demonstrates that the M210 platform instrumentation provides an

524   accurate, albeit less precise representation of the atmosphere.

525

A)

543
544

B)
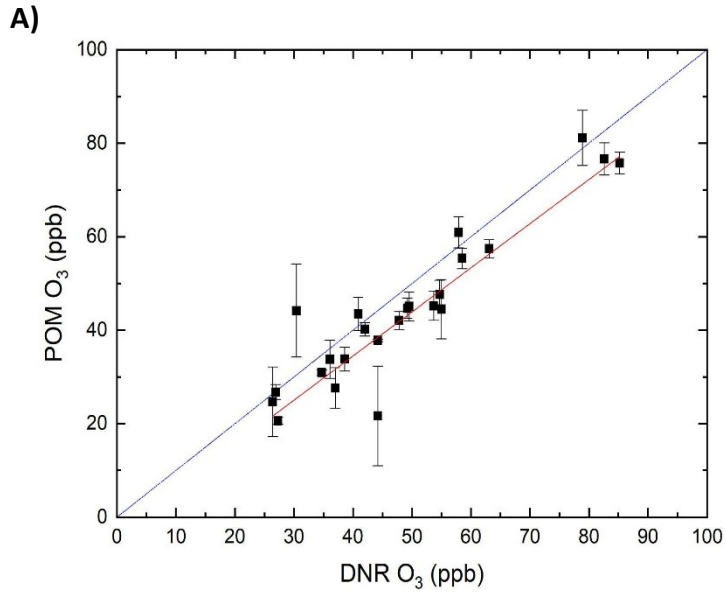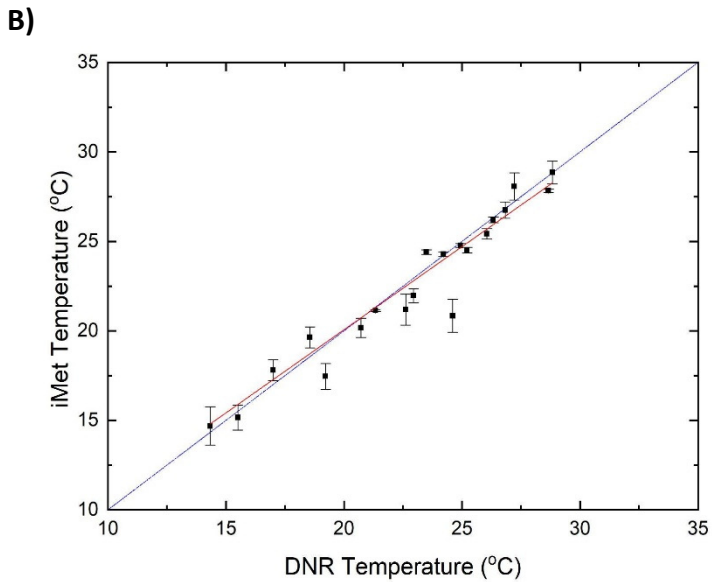
Figure 10: Intercomparsion between measurements from instrumentation on the M210 at 5 m AGL and at the WI-DNR ground station for a) O_3 (ppb) observations and b) temperature (º C). Blue lines depict 1:1 agreement and red lines depict the linear regression best fit with a) $O_{3\ (POM)} = 0.944\ (\pm\ 0.044)\ O_{3\ (DNR)} - 3.3\ (\pm1.9)$, $R^2 = 0.955$, and b) $T_{iMET} = 0.929(\pm\ 0.038)\ T_{DNR} + 1.48(\pm0.93)$, $R^2 = 0.970$.

5. Data Availability and File Structure

A community data repository has been established for this field campaign at https://zenodo.org/communities/wiscodisco21/. The data sets in the repository cover the merged iMET and POM data sets from the M210 (DOI:10.5281/zenodo.5160346) as .txt files, the RAAVEN dataset (DOI: 10.5281/zenodo.5142491) as .cdf files, and the doppler lidar wind profiler (DOI: 10.5281/zenodo.5213039) as .cdf files. M210 files have a naming convention that includes WiscoDisco_M210_YYYYMMDD_F#, where the flight number for the day is indicated by F#. RAAVEN files have a naming convention that includes WiscoDisco_CU-RAAVEN_YYYYMMDD_hhmmss_B1.nc, where YYYYMMDD is the year, month and day that the data were collected, hhmmss is the time of power on for the aircraft, and B1 is the data processing level, where B1 files have had data quality checks and post-processing (e.g. coldwire calibration and wind estimation) applied. The Doppler lidar files have a naming convention that includes chiwaukee_wind_profiles_YYYYMMDD and chiwaukee_stare_YYYYMMDD. All datasets include geospatial information (latitude, longitude, altitude) and timestamps in UTC.

6. Interpreted Results

The WiscoDISCO-21 project demonstrates how UAS can be used to sample a complex circulation near to the surface without causing major disruption to people, wildlife and ecosystems in the area. An example of a characterization of lake breeze incursion is shown in Figures 11 and 12, which include the temperature profiles from the M210 and RAAVEN (Fig. 11) and Doppler lidar u wind component (Fig. 12). The temperature profiles from the M210 and RAAVEN show a notable temperature inversion in the late afternoon below 150 m and the Doppler lidar u wind component shows easterly winds arriving after 18:00 UTC. The combination of u component winds from Doppler lidar and the temperature observations from the UAS platforms are consistent in demonstrating a marine layer incursion with maximum height of approximately 250 m AGL at 21:00 UCT collapsing to a height of 100 m AGL by 22:00 UTC. The nonuniform start to the lake breeze onset fluctuated, shown as shifting u component winds from easterly to westerly after 18:00 UTC (Fig. 12) and disagreement with the lowest altitude observations from the M210 and RAAVEN between 18:30-19:00 UTC (Fig. 11). The distance between the M210 launch site

594   and the RAAVEN landing site complicates the low altitude observations of temperatures between 18:00

595   and 19:00 UTC, which also may indicate the very limited incursion of the lake breeze at that time.
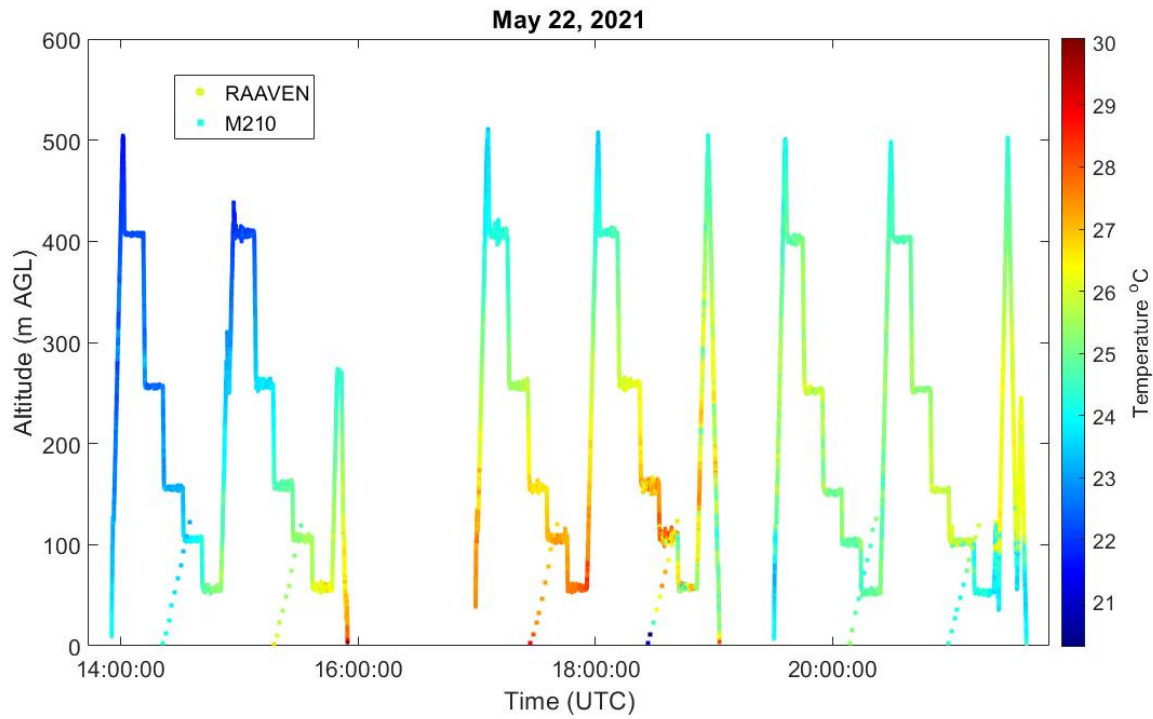
596

597

598   **Figure 11**: Temperatures (^{o} C) measured from University of Colorado RAAVEN (O) and the M120 (□)
599   on May 22, 2021. RAAVEN was flying over-prairie circular spirals Pattern A.

600
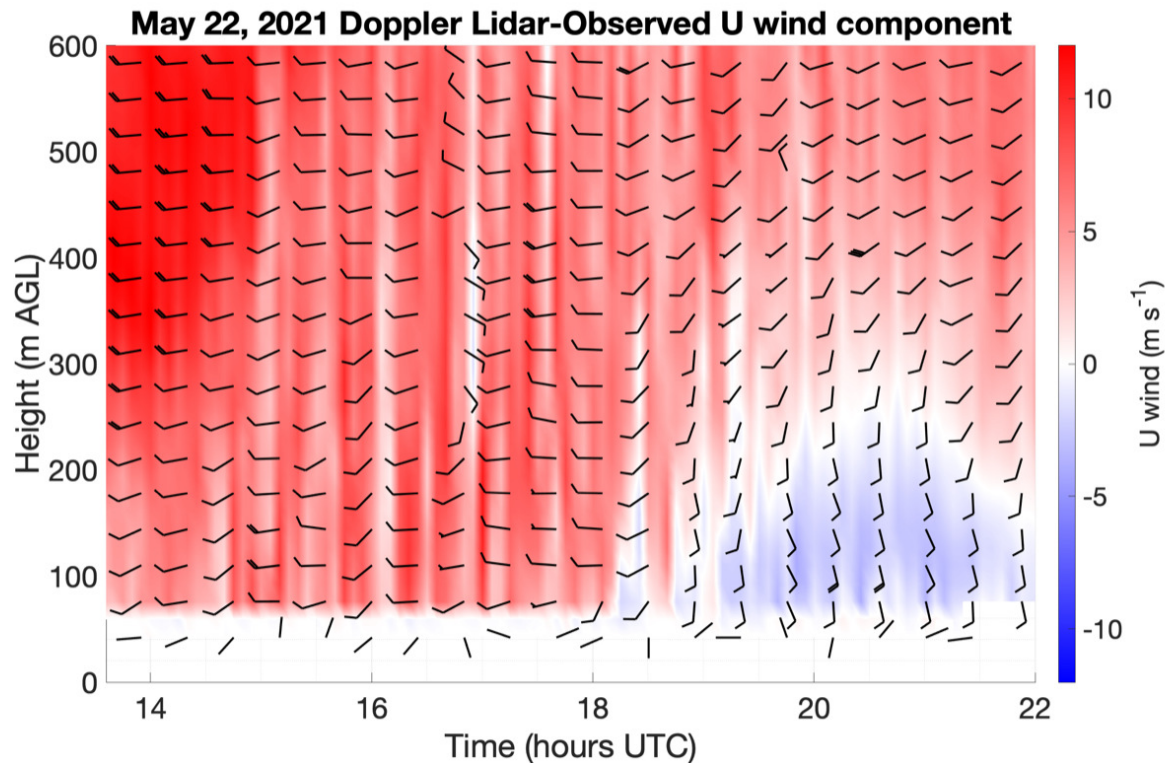
Figure 12: Time/height cross section of the u (zonal) component of the Doppler lidar-observed
horizontal winds (in m/s), overlaid with horizontal wind barbs (in kts) plotted according to the standard
convention from May 22, 2021. Wind barbs are thinned by a factor of five in the time dimension and a
factor of two in the height dimension to aid readability.

7. Summary

The 2021 WiscoDISCO field campaign incorporated the use of two UAS platforms for meteorological

and chemical measurements in the atmosphere, a multirotor completing vertical profiles up to 120 m AGL

and a fixed wing executing flight patterns up to 500 m AGL alongside a Lidar WindPro instrument

capable of sensing winds and aerosol backscatter from altitudes of 100-2000 m AGL. The overlapping

domains are useful for characterizing low altitude mesoscale meteorology of the lake breeze at a shoreline

environment that regularly observes ozone enhancement events during onshore flow. Data from all

instruments and platforms have been compiled, quality-control tested and uploaded to a community

repository. The collaborative field campaign involved teams from 4 different universities and obtained

615 continuous lidar data in conjunction with 24 flight hours of fixed wing and 6 flight hours of multi-rotor

616 vertical profiles on days likely impacted by lake breeze.

617

618 The data from the WiscoDISCO-21 campaign can be used to evaluate the markers for lake breeze

619 incursion overland in winds, temperatures, chemical composition and optical properties (backscatter).

620 The thermodynamic conditions for lake breeze incursion at a local scale can be determined through the

621 evaluation of horizontal and vertical winds, atmospheric stability and potential temperature. The

622 positioning of pollutants with respect to the marine layer markers can also be investigated.

623

624 **Author Contributions.**

625 Patricia A. Cleary is the PI of this project and was responsible for data collection, overseeing data analysis

626 from the M210, field campaign planning and logistics, and the writing and editing of this document. Ben

627 Kies was responsible for data collection for the M210 in the field, Joe Tirado was responsible for data

628 analysis, quality control and data formatting for the repository for the M210, Aidan Voon was responsible

629 for data analysis for the M210. Joe Hupy was responsible for piloting the M210 and the writing and

630 editing of this paper. Gijs de Boer was responsible for coordination and execution of the University of

631 Colorado RAAVEN flights, and for development, writing and editing of the publication. Steve Borenstein

632 and Jonathan Hamilton contributed to the collection of the RAAVEN dataset as field operators, and

633 supported the development of this manuscript. Dale Lawrence supplied instrumentation for the RAAVEN

634 UAS and contributed to the writing of the manuscript. Tim Wagner and R Bradley Pierce were

635 responsible for data collection, data analysis of the doppler lidar instrumentation, and writing and editing

636 this document and R Bradley Pierce assisted in field planning.

637
638
639 **Competing Interests.**

640 GB works as a consultant for Black Swift Technologies, who manufacture the multi-hole pressure probe

641 used in the collection of the RAAVEN dataset.

642
643
644 **Acknowledgements**.

This material is based upon work funded by the National Science Foundation award #1918850. The UW-Eau Claire team acknowledges support from the Student Blugold Commitment Differential Tuition program. The University of Colorado team acknowledges financial support from the University of Wisconsin Eau-Claire through a sub-contract supported by the US National Science Foundation, as well as support from the NOAA Physical Sciences Laboratory. Any opinions, findings, and conclusions or recommendations expressed in this material are those of the author(s) and do not necessarily reflect the views of the National Science Foundation. The authors thank Nathan Taminger and Paul McKinley for their participation in the WiscDISCO-21 field campaign.

References

Abdi-Oskouei, M., Carmichael, G., Christiansen, M., Ferrada, G., Roozitalab, B., Sobhani, N., Wade, K., Czarnetzki, A., Pierce, R. B., Wagner, T., and Stanier, C.: Sensitivity of Meteorological Skill to Selection of WRF-Chem Physical Parameterizations and Impact on Ozone Prediction During the Lake Michigan Ozone Study (LMOS), Journal of Geophysical Research-Atmospheres, 125, 25, 10.1029/2019jd031971, 2020.

Brown, E. N., Friehe, C. A., and Lenschow, D. H.: THE USE OF PRESSURE-FLUCTUATIONS ON THE NOSE OF AN AIRCRAFT FOR MEASURING AIR MOTION, Journal of Climate and Applied Meteorology, 22, 171-180, 10.1175/1520-0450(1983)022<0171:Tuopfo>2.0.Co;2, 1983.

Caicedo, V., Delgado, R., Luke, W. T., Ren, X. R., Kelley, P., Stratton, P. R., Dickerson, R. R., Berkoff, T. A., and Gronoff, G.: Observations of bay-breeze and ozone events over a marine site during the OWLETS-2 campaign, Atmospheric Environment, 263, 10.1016/j.atmosenv.2021.118669, 2021.

Cleary, P. A., Fuhrman, N., Schulz, L., Schafer, J., Fillingham, J., Bootsma, H., McQueen, J., Tang, Y., Langel, T., McKeen, S., Williams, E. J., and Brown, S. S.: Ozone distributions over southern Lake Michigan: comparisons between ferry-based observations, shoreline-based DOAS observations and model forecasts, Atmospheric Chemistry and Physics, 15, 5109-5122, 10.5194/acp-15-5109-2015, 2015.

Cleary, P. A., Dickens, A. J., McIlquham, M., Sanchez, M., Geib, K., Hedberg, C., Hupy, J., Watson, M. W., Fuoco, M., Olson, E. R., Pierce, R. B., Stanier, C., Long, R., Valin, L., Conley, S., and Smith, M.: Impacts of lake breeze meteorology on ozone gradient observations along Lake Michigan Shorelines in Wisconsin: 2017 LMOS examples in press, Atmospheric Environment, 2022.

de Boer, G., Borenstein, S., Hamilton, J., Osborn, J., Lawrence, D., Argrow, B., and Intrieri, J.: Measurements from the University of Colorado RAAVEN Uncrewed Aircraft System during ATOMIC, Earth System Science Data, submitted, 2021a.

de Boer, G., Elston, J., Houston, A., Pillar-Little, E., Argrow, B., Bell, T., Chilson, P., Choate, C., Greene, B., Islam, A., Detweiler, C., Jacob, J., Natalie, V., Rhodes, M., Rico, D., Stachura, M., Lappin, F., Whyte, S., and Wilson, M.: Evaluation and Intercomparison of Small Uncrewed Aircraft Systems

682 Used for Atmospheric Research, in preparation, Journal of Atmospheric and Oceanic Technology,
683 2021b.
684 Doak, A. G., Christiansen, M. B., Alwe, H. D., Bertram, T. H., Carmichael, G., Cleary, P., Czarnetzki,
685 A. C., Dickens, A. F., Janssen, M., Kenski, D., Millet, D. B., Novak, G. A., Pierce, B. R., Stone, E. A.,
686 Long, R. W., Vermeuel, M. P., Wagner, T. J., Valin, L., and Stanier, C. O.: Characterization of ground-
687 based atmospheric pollution and meteorology sampling stations during the Lake Michigan Ozone Study
688 2017, Journal of the Air & Waste Management Association, 71, 866-889,
689 10.1080/10962247.2021.1900000, 2021.
690 Dye, T. S., Roberts, P. T., and Korc, M. E.: Observations of transport processes for ozone and ozone
691 precursors during the 1991 Lake Michigan Ozone Study, Journal of Applied Meteorology, 34, 1877-
692 1889, 10.1175/1520-0450(1995)034<1877:ootpfo>2.0.co;2, 1995.
693 Elston, J., Argrow, B., Stachura, M., Weibel, D., Lawrence, D., and Pope, D.: Overview of Small Fixed-
694 Wing Unmanned Aircraft for Meteorological Sampling, Journal of Atmospheric and Oceanic
695 Technology, 32, 97-115, 10.1175/jtech-d-13-00236.1, 2015.
696 Foley, T., Betterton, E. A., Jacko, P. E. R., and Hillery, J.: Lake Michigan air quality: The 1994-2003
697 LADCO Aircraft Project (LAP), Atmospheric Environment, 45, 3192-3202,
698 10.1016/j.atmosenv.2011.02.033, 2011.
699 Frew, E. W., Argrow, B., Borenstein, S., Swenson, S., Hirst, C. A., Havenga, H., and Houston, A.: Field
700 observation of tornadic supercells by multiple autonomous fixed-wing unmanned aircraft, Journal of
701 Field Robotics, 37, 1077-1093, 10.1002/rob.21947, 2020.
702 Geddes, J. A., Wang, B., and Li, D.: Ozone and Nitrogen Dioxide Pollution in a Coastal Urban
703 Environment: The Role of Sea Breezes, and Implications of Their Representation for Remote Sensing
704 of Local Air Quality, Journal of Geophysical Research-Atmospheres, 126, 10.1029/2021jd035314,
705 2021.
706 Gronoff, G., Robinson, J., Berkoff, T., Swap, R., Farris, B., Schroeder, J., Halliday, H. S., Knepp, T.,
707 Spinei, E., Carrion, W., Adcock, E. E., Johns, Z., Allen, D., and Pippin, M.: A method for quantifying
708 near range point source induced O-3 titration events using Co-located Lidar and Pandora measurements,
709 Atmospheric Environment, 204, 43-52, 10.1016/j.atmosenv.2019.01.052, 2019.
710 Guimaras, P., Ye, J. H., Batista, C., Barbosa, R., Ribeiro, I., Medeiros, A., Zhao, T. N., Hwang, W. C.,
711 Hung, H. M., Souza, R., and Martin, S. T.: Vertical Profiles of Atmospheric Species Concentrations and
712 Nighttime Boundary Layer Structure in the Dry Season over an Urban Environment in Central Amazon
713 Collected by an Unmanned Aerial Vehicle, Atmosphere, 11, 10.3390/atmos11121371, 2020.
714 Hayden, K. L., Sills, D. M. L., Brook, J. R., Li, S. M., Makar, P. A., Markovic, M. Z., Liu, P., Anlauf,
715 K. G., O'Brien, J. M., Li, Q., and McLaren, R.: Aircraft study of the impact of lake-breeze circulations
716 on trace gases and particles during BAQS-Met 2007, Atmospheric Chemistry and Physics, 11, 10173-
717 10192, 10.5194/acp-11-10173-2011, 2011.
718 Holton, J.: An Introduction to Dynamic Meteorology, third ed., Academic Press, San Diego1992.
719 Horel, J., Crosman, E., Jacques, A., Blaylock, B., Arens, S., Long, A., Sohl, J., and Martin, R.: Summer
720 ozone concentrations in the vicinity of the Great Salt Lake, Atmospheric Science Letters, 17, 480-486,
721 10.1002/asl.680, 2016.

722   Jozef, G., Cassano, J., Dahlke, S., and de Boer, G.: Testing the efficacy of boundary layer height
723   detection algorithms using uncrewed aircraft system data from MOSAIC, Atmos. Meas. Tech.,
724   submitted.
725   Keen, C. S. and Lyons, W. A.: Lake/Land Breeze circulations on the western shore of Lake Michigan,
726   Journal of Applied Meteorology, 17, 1843-1855, 10.1175/1520-0450(1978)017<1843:lbcotw>2.0.co;2,
727   1978.
728   Lennartson, G. J. and Schwartz, M. D.: The lake breeze-ground-level ozone connection in eastern
729   Wisconsin: A climatological perspective, International Journal of Climatology, 22, 1347-1364,
730   10.1002/joc.802, 2002.
731   Levy, I., Makar, P. A., Sills, D., Zhang, J., Hayden, K. L., Mihele, C., Narayan, J., Moran, M. D.,
732   Sjostedt, S., and Brook, J.: Unraveling the complex local-scale flows influencing ozone patterns in the
733   southern Great Lakes of North America, Atmospheric Chemistry and Physics, 10, 10895-10915,
734   10.5194/acp-10-10895-2010, 2010.
735   Lyons, W. A. and Cole, H. S.: Photochemical oxidant transport - Mesoscale lake breeze and synoptic-
736   scale aspects, Journal of Applied Meteorology, 15, 733-743, 10.1175/1520-
737   0450(1976)015<0733:potmlb>2.0.co;2, 1976.
738   Lyons, W. A. and Olsson, L. E.: Detailed mesometeorological studies of air pollution dispersion in
739   Chicago lake breeze, Monthly Weather Review, 101, 387-403, 10.1175/1520-
740   0493(1973)101<0387:dmsoap>2.3.co;2, 1973.
741   Martin, J. E.: Mid-Latitude Atmospheric Dynamics: A First Course, John Wiley & Sons, West
742   Sussex2006.
743   McNider, R. T., Pour-Biazar, A., Doty, K., White, A., Wu, Y. L., Qin, M. M., Hu, Y. T., Odman, T.,
744   Cleary, P., Knipping, E., Dornblaser, B., Lee, P., Hain, C., and McKeen, S.: Examination of the
745   Physical Atmosphere in the Great Lakes Region and Its Potential Impact on Air QualityOverwater
746   Stability and Satellite Assimilation, Journal of Applied Meteorology and Climatology, 57, 2789-2816,
747   10.1175/jamc-d-17-0355.1, 2018.
748   Miller, S. T. K., Keim, B. D., Talbot, R. W., and Mao, H.: Sea breeze: Structure, forecasting, and
749   impacts, Reviews of Geophysics, 41, 10.1029/2003rg000124, 2003.
750   Qin, M. M., Yu, H. F., Hu, Y. T., Russell, A. G., Odman, M. T., Doty, K., Pour-Biazar, A., McNider, R.
751   T., and Knipping, E.: Improving ozone simulations in the Great Lakes Region: The role of emissions,
752   chemistry, and dry deposition, Atmospheric Environment, 202, 167-179,
753   10.1016/j.atmosenv.2019.01.025, 2019.
754   Sills, D. M. L., Brook, J. R., Levy, I., Makar, P. A., Zhang, J., and Taylor, P. A.: Lake breezes in the
755   southern Great Lakes region and their influence during BAQS-Met 2007, Atmospheric Chemistry and
756   Physics, 11, 7955-7973, 10.5194/acp-11-7955-2011, 2011.
757   Stanier, C. O., Pierce, R. B., Abdi-Oskouei, M., Adelman, Z. E., Al-Saadi, J., Alwe, H. D., Bertram, T.
758   H., Carmichael, G. R., Christiansen, M. B., Cleary, P. A., Czarnetzki, A. C., Dickens, A. F., Fuoco, M.
759   A., Hughes, D. D., Hupy, J. P., Janz, S. J., Judd, L. M., Kenski, D., Kowalewski, M. G., Long, R. W.,
760   Millet, D. B., Novak, G., Roozitalab, B., Shaw, S. L., Stone, E. A., Szykman, J., Valin, L., Vermeuel,
761   M., Wagner, T. J., and Whitehill, A. R.: Overview of the Lake Michigan Ozone Study 2017, Bulletin of
762   the American Meteorological Society, doi.org/10.1175/BAMS-D-20-0061.1, 2021.

763 Vermeuel, M. P., Novak, G. A., Alwe, H. D., Hughes, D. D., Kaleel, R., Dickens, A. F., Kenski, D.,
764 Czarnetzki, A. C., Stone, E. A., Stanier, C. O., Pierce, R. B., Millet, D. B., and Bertram, T. H.:
765 Sensitivity of Ozone Production to NOx and VOC Along the Lake Michigan Coastline, Journal of
766 Geophysical Research-Atmospheres, 124, 10989-11006, 10.1029/2019jd030842, 2019.
767 Wagner, T. J., Klein, P. M., and Turner, D. D.: A NEW GENERATION OF GROUND-BASED
768 MOBILE PLATFORMS FOR ACTIVE AND PASSIVE PROFILING OF THE BOUNDARY LAYER,
769 Bulletin of the American Meteorological Society, 100, 137-153, 10.1175/bams-d-17-0165.1, 2019.
770 Wagner, T. J., Czarnetzki, A. C., Christiansen, M., Pierce, R. B., Stanier, C. O., Dickens, A. F., and
771 Eloranta, E. W.: Observations of the Development and Vertical Structure of the Lake Breeze
772 Circulation During the 2017 Lake Michigan Ozone Study, Submitted, 2021.
773 Wagner, T. J., Czarnetzki, A. C., Christiansen, M., Pierce, R. B., Stanier, C. O., Dickens, A. F., and
774 Eloranta, E. W.: Observations of the Development and Vertical Structure of the Lake Breeze
775 Circulation During the 2017 Lake Michigan Ozone Study, Journal of the Atmospheric Sciences,
776 https://doi.org/10.1175/JAS-D-20-0297.1, 2022.
777 Wentworth, G. R., Murphy, J. G., and Sills, D. M. L.: Impact of lake breezes on ozone and nitrogen
778 oxides in the Greater Toronto Area, Atmospheric Environment, 109, 52-60,
779 10.1016/j.atmosenv.2015.03.002, 2015.
780 Wildmann, N., Ravi, S., and Bange, J.: Towards higher accuracy and better frequency response with
781 standard multi-hole probes in turbulence measurement with remotely piloted aircraft (RPA),
782 Atmospheric Measurement Techniques, 7, 1027-1041, 10.5194/amt-7-1027-2014, 2014.
783